Modeling the optical constants of Al x Ga 1−x As alloys

Aleksandra B. Djurišić, Aleksandar D. Rakić, Paul C. K. Kwok, E. Herbert Li, Marian L. Majewski, and Jovan M. Elazar

Articles you may be interested in

Calculations of the temperature and alloy composition effects on the optical properties of Al x Ga 1 − x As y Sb 1 − y and Ga x In 1 − x As y Sb 1 − y in the spectral range 0.5–6 eV
J. Appl. Phys. **102**, 014504 (2007); 10.1063/1.2751406

Modeling the optical constants of GaP, InP, and InAs
J. Appl. Phys. **85**, 3638 (1999); 10.1063/1.369727

The optical constants of n- and p-doped In 0.66 Ga 0.34 As on InP (001) including the Burstein-Moss shift: Experiment and modeling
AIP Conf. Proc. **460**, 39 (1999); 10.1063/1.57820

Optical constants of (Al 0.98 Ga 0.02) x O y native oxides
Appl. Phys. Lett. **73**, 3512 (1998); 10.1063/1.122821

Optical constants and electronic interband transitions of disordered GaAs 1−x P x alloys
J. Appl. Phys. **84**, 3696 (1998); 10.1063/1.368546

Modeling the optical constants of Al$_x$Ga$_{1-x}$As alloys

Aleksandra B. Djurišić
*Department of Electrical and Electronic Engineering, University of Hong Kong, Pokfulam Road,
Hong Kong*

Aleksandar D. Rakić
*Department of Computer Science and Electrical Engineering, The University of Queensland,
Brisbane QLD 4072, Australia*

Paul C. K. Kwok and E. Herbert Li[a]
*Department of Electrical and Electronic Engineering, University of Hong Kong, Pokfulam Road,
Hong Kong*

Marian L. Majewski
*Department of Computer Science and Electrical Engineering, The University of Queensland,
Brisbane QLD 4072, Australia*

Jovan M. Elazar
School of Electrical Engineering, Unniversity of Belgrade, PO Box 35-54, Belgrade, Yugoslavia

The extension of Adachi's model with a Gaussian-like broadening function, in place of Lorentzian, is used to model the optical dielectric function of the alloy Al$_x$Ga$_{1-x}$As. Gaussian-like broadening is accomplished by replacing the damping constant in the Lorentzian line shape with a frequency dependent expression. In this way, the comparative simplicity of the analytic formulas of the model is preserved, while the accuracy becomes comparable to that of more intricate models, and/or models with significantly more parameters. The employed model accurately describes the optical dielectric function in the spectral range from 1.5 to 6.0 eV within the entire alloy composition range. The relative rms error obtained for the refractive index is below 2.2% for all compositions. © *1999 American Institute of Physics.* [S0021-8979(99)00512-5]

I. INTRODUCTION

The alloy system Al$_x$Ga$_{1-x}$As/GaAs is of great technological importance in the fabrication of various optoelectronic devices. In the design and analysis of these devices, the refractive index and absorption coefficient of the material have to be known over a wide range of wavelengths. Optical properties of a solid are often described in terms of the complex dielectric function $\epsilon(\omega) = \epsilon_1(\omega) + \epsilon_2(\omega)$ [or the complex index of refraction $N(\omega) = n(\omega) + ik(\omega)$]. Aspnes *et al.*[1] have measured the optical properties of Al$_x$Ga$_{1-x}$As alloys at room temperature by spectroscopic ellipsometry for energies from 1.5 to 6.0 eV and compositions $x = 0.0–0.8$ in steps of 0.1. There have also been several experimental studies of pure materials—GaAs[2,3] and AlAs.[4–7] However, the significant shortcomings of these experimental studies are that the data are not expressed in terms of continuous analytical functions of the electronic energy gaps and the alloy composition x. Therefore, there is a requirement to model the experimental data with an analytical model. The model employed must be simple and concise, giving a reasonably good approximation of the optical spectra of investigated materials at the same time.

In modeling the dispersion adequately below the direct band gap, a simple, single-effective oscillator model of Wemple and DiDomenico[8,9] can be used. The direct absorp-

tion edge E_0 is taken into account in the model proposed by Afromowitz[10] and its recent modifications.[11,12] This model gives reasonable agreement with the experiment for low energies, and it has been frequently used for device-designing purposes.[13–18] Erman *et al.*[19] propose a phenomenological model based on a damped harmonic oscillator (DHO) approximation, which has been used to calculate the optical dielectric function at energies above E_0. Terry[20] proposed a modification of the DHO model by introducing an independent phase for each oscillator. He used nine oscillators to obtain a good quality fit (relative rms error for refractive index is <0.03 for all compositions), although there were still some inaccuracies around E_0, especially for compositions $x = 0.198$ and $x = 0.315$. The oscillator parameters were assumed to be the cubic functions of composition x, thus giving a total of $4 \times 36 = 144$ model parameters.

Adachi's model[21,22] is a relatively simple model which describes the optical dielectric function with terms attributed to four energy gaps (E_0, $E_0 + \Delta_0$, E_1, $E_1 + \Delta_1$) and damped harmonic oscillators describing the contributions from higher lying transitions [E_0', $E_2(X)$, $E_2(\Sigma)$]. However, Adachi's model is not very accurate, and several modifications have been proposed recently.[3,23–28,34] Jenkins[24] has obtained better agreement with the experimental data by introducing an exponential decay of matrix elements which are taken to be constant over the Brillouin zone in Adachi's model. Nonetheless, this model gives good agreement with the experi-

mental data only in the narrow range, and for AlAs, the calculated values differ from the experimental ones for a constant amount below 3 eV. Zheng, Lin, and Kuo[28] have recently proposed a modification of Adachi's model which includes excitonic terms at E_1 and $E_1 + \Delta_1$. They also give a new expression for the contribution of the indirect energy gap, and introduce the Lorentzian lifetime broadening in a different way. However, since the model parameters (except the fundamental band gap) are assumed to be linear functions of composition, this model does not yield a good agreement with the experimental data for alloys of higher aluminum content ($x \geq 0.7$).

Kim *et al.*[29–31] have proposed an accurate but rather complicated model, which can include either Lorentzian or Gaussian broadening. Different types of broadening can be accomplished by varying a certain parameter in the expression for the frequency dependent damping constant. The experimental data for $Al_xGa_{1-x}As$ in the energy range from 1.5 to 6.0 eV and compositions from $x = 0.0$ to $x = 0.8$ (in steps 0.1) and $x = 1$ are fitted with 119 parameters. The relative rms error obtained for the refractive index using this model is below 2.5% for all compositions.[30]

The model of Kim *et al.*[30] is much more complex than Adachi's model and contains a large number of adjustable parameters. The improvement in accuracy, however, is obtained mainly through replacing the Lorentzian broadening function with the Gaussian one. This model does not provide a good agreement with the experiment in the vicinity of the direct edge and below when using a simple Lorentzian broadening function. The fact that Lorentzian broadening does not accurately describe the optical spectrum has already been recognized and discussed.[29,32–34] Rakić and Majewski[34] have shown that Adachi's model with the Gaussian-like broadening function accurately describes the dispersion and absorption of GaAs and AlAs even in the vicinity of the E_0, where the original model of Ozaki and Adachi[3] is highly inaccurate.

In this article, we show that a comparatively simple model of Rakić and Majewski[34] can be successfully applied to model the optical spectrum of ternary alloys, in particular $Al_xGa_{1-x}As$, with an accuracy similar to that of the significantly more intricate model of Kim *et al.*[30] The main aim of modeling the optical properties of a ternary alloy is to enable the calculation of the optical constants for compositions with no available experimental data. We present here a method for the accurate and reliable determination of model parameters as a function of content x. We compare two ways to determine the model parameters for ternary compounds. The first approach is to determine the model parameters for particular compositions, and then to find the optimal function describing the dependence of the model parameters on the alloy composition x. The second approach is to simultaneously fit the data sets for all available compositions and energies in order to minimize the discrepancies between the calculated and experimental data over the entire energy and composition ranges. Our results clearly show that this simultaneous fitting is needed to provide accurate values of optical functions. Finally, we discuss the advantages of using the global optimizing routine (namely our acceptance-probability-

controlled simulated annealing algorithm[35,36]) instead of using classical fitting algorithms, and also how it effects the reliability of the final model parameters.

In the following section, a description of the employed model is presented. In Sec. III, the model parameters of the alloy $Al_xGa_{1-x}As$ as a function of content x are determined and a discussion given. Section IV sets out the conclusions.

II. MODEL OF THE DIELECTRIC FUNCTION

The following is a brief summary describing the applied model for the dielectric function. The dielectric function in Adachi's model is represented by the sum of terms describing transitions at critical points (CPs) in the joint density of states. In the modification proposed by Rakić and Majewski,[34] damping constants Γ_i are replaced with the frequency dependent expression $\Gamma_i'(\omega)$.

A. E_0 and $E_0 + \Delta_0$ transitions

Under the parabolic band assumption, contributions of three-dimensional M_0 CPs, E_0, and $E_0 + \Delta_0$ are given by[3]

$$\epsilon^{\mathrm{I}}(\omega) = A E_0^{-3/2} \left[f(\chi_0) + \frac{1}{2} \left(\frac{E_0}{E_0 + \Delta_0} \right)^{3/2} f(\chi_{0s}) \right] \quad (1)$$

with

$$f(y) = y^{-2} [2 - (1+y)^{1/2} - (1-y)^{1/2}], \quad (2)$$

$$\chi_0 = \frac{\hbar\omega + i\Gamma_0}{E_0}, \quad (3)$$

$$\chi_{0s} = \frac{\hbar\omega + i\Gamma_0}{E_0 + \Delta_0}, \quad (4)$$

where A and Γ_0 are the strength and damping constants of the E_0 and $E_0 + \Delta_0$ transition, respectively.

B. E_1 and $E_1 + \Delta_1$ transitions

Adachi[3] obtains the following expression for the contributions of the two-dimensional M_0 CPs, E_1 and $E_1 + \Delta_1$. He assumed the matrix element to be constant with respect to energy

$$\epsilon^{\mathrm{II}}(\omega) = -B_1\chi_1^{-2}\ln(1-\chi_1^2) - B_{1s}\chi_{1s}^{-2}\ln(1-\chi_{1s}^2), \quad (5)$$

where

$$\chi_1 = \frac{\hbar\omega + i\Gamma_1}{E_1}, \quad (6)$$

$$\chi_{1s} = \frac{\hbar\omega + i\Gamma_1}{E_1 + \Delta_1}. \quad (7)$$

$B_1(B_{1s})$ and Γ_1 are the strength and damping constant of the E_1 and $E_1 + \Delta_1$ transitions, respectively. The contribution of the Wannier-type two-dimensional excitons (a discrete series of exciton lines at the E_1 and $E_1 + \Delta_1$ CPs) is given by[3]

$$\epsilon^{\mathrm{III}}(\omega) = \sum_{n=1}^{+\infty} \frac{1}{(2n-1)^3} \left(\frac{B_{1x}}{E_1 - [G_1/(2n-1)^2] - \hbar\omega - i\Gamma_1} \right.$$

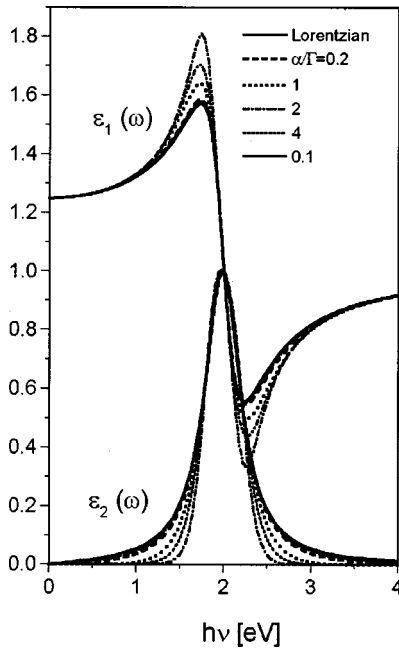$$\left. + \frac{B_{2x}}{(E_1 + \Delta_1) - [G_{1s}/(2n-1)^2] - \hbar\omega - i\Gamma_1} \right), \quad (8)$$

FIG. 1. Illustration of the influence of frequency dependent damping on optical constants.

TABLE I. Parameters describing composition dependence of the four lowest critical points E_0, $E_0+\Delta_0$, E_1, and $E_1+\Delta_1$ according to Kim *et al.* (see Ref. 30). All parameters are in eV.

Parameter	$E(0)$	$E(1)-E(0)$	c_0	c_1
E_0	1.410	1.583	0.2242	−1.4235
$E_0+\Delta_0$	1.746	1.455	0.1931	−1.2160
E_1	2.926	0.962	−0.2124	−0.7850
$E_1+\Delta_1$	3.170	0.917	−0.0734	−0.9393

where B_{1x} and B_{2x} are the strengths, and G_1 and G_{1s} are Rydberg energies of E_1 and $E_1+\Delta_1$ excitons, respectively. Here, it is assumed that $G_1=G_{1s}=0$.[3,34] Summation of the excitonic terms is performed until the contribution of the next term is less than 10^{-4}.

C. E_0', $E_2(X)$ and $E_2(\Sigma)$ transitions

The origin of transitions E_0', $E_2(X)$, and $E_2(\Sigma)$ is not completely clear, since they do not correspond to a single, well defined CP. However, these features can be adequately modeled with damped harmonic oscillators, which are characterized by energy E_j, oscillator strength $f_j=\sqrt{C_j E_j^2}$, and damping constant Γ_j, $j=2,3,4$[3]

$$\epsilon^{IV}(\omega)=\sum_{j=2}^{4}\frac{f_j^2}{E_j^2-(\hbar\omega)^2-i\hbar\omega\Gamma_j}. \qquad (9)$$

D. The frequency dependent damping

When the damping constants in Eqs. (1)–(9) are replaced with[34]

$$\Gamma_i'(\omega)=\Gamma_i\exp\left[-\alpha_i\left(\frac{\hbar\omega-E_i}{\Gamma_i}\right)^2\right], \qquad (10)$$

the shape of the line varies with the ratio of parameters α_j and Γ_j. This is illustrated in Fig. 1, where the real and imaginary parts of the optical dielectric function of a single damped harmonic oscillator [calculated according to Eq. (9), with the damping constant replaced with Eq. (10)] versus energy for several different ratios α_j/Γ_j, is shown. Line shapes range from purely Lorentzian (for $\alpha=0$) to nearly Gaussian ($\alpha=0.3$), while for large values of the ratio α_j/Γ_j, the wings of the line in the imaginary part of the dielectric function $\epsilon_2(\omega)$ are even narrower. This enables the

elimination of extended absorption tails in ϵ_2, which are characteristic of Lorentzian line shape. Since no broadening mechanism is set *a priori* (both α_j and Γ_j are adjustable model parameters), this then makes the model very flexible.

E. Complete model for the dielectric function

The dielectric function is obtained by summing up the contributions of all the CPs as described above. Γ is replaced by $\Gamma'(\omega)$

$$\epsilon(\omega)=\epsilon_{1\infty}+\epsilon^{I}(\omega)+\epsilon^{II}(\omega)+\epsilon^{III}(\omega)+\epsilon^{IV}(\omega), \qquad (11)$$

where $\epsilon_{1\infty}$ is the dielectric constant arising from the contributions of higher lying transitions.

III. RESULTS AND DISCUSSION

The positions of the E_0, $E_0+\Delta_0$, E_1, and $E_1+\Delta_1$ and their variations with composition x are accurately determined in the study of Kim *et al.*[30] The energies of these CPs are given by

$$E_i(x)=E_i(0)+[E_i(1)-E_i(0)]x+(c_0+c_1x)x(1-x), \qquad (12)$$

where the values of $E_i(0)$, $E_i(1)$, c_0, and c_1 are listed in Table I. As a result of using Eq. (12) the CP energies can be represented without any further adjustment of the parameters of the model. For other model parameters, each parameter is assumed to be a cubic polynomial of alloy composition x, having the form $a_{0i}(1-x)+a_{1i}x+(a_{2i}+a_{3i}x)x(1-x)$. No attempt has been made to constrain the values during the fitting procedure, except that the algorithm restricts the parameter values to be always positive. The following objective function is employed:

$$F=\sum_{j=1}^{j=N_x}\sum_{i=1}^{i=N_p}\left[\left|\frac{\epsilon_1(\omega_i,x_j)-e_1^{\text{expt}}(\omega_i,x_j)}{\epsilon_1^{\text{expt}}(\omega_i,x_j)}\right|\right.$$
$$\left.+\left|\frac{\epsilon_2(\omega_i,x_j)-\epsilon_2^{\text{expt}}(\omega_i,x_j)}{\epsilon_2^{\text{expt}}(\omega_i,x_j)}\right|\right]^2, \qquad (13)$$

where N_p is the number of experimental points, N_x is the number of different alloy compositions, and $\epsilon_1(\omega_i,x_j)$, $\epsilon_2(\omega_i,x_j)$ are calculated values of the real and imaginary parts of the dielectric constant at frequency ω_i for composition x_j. The corresponding experimental values are $\epsilon_1^{\text{expt}}(\omega_i,x_j)$ and $\epsilon_2^{\text{expt}}(\omega_i,x_j)$. The objective function is minimized using the acceptance probability controlled simulated annealing algorithm with the adaptive move-generation procedure, as is described in detail in Ref. 35.
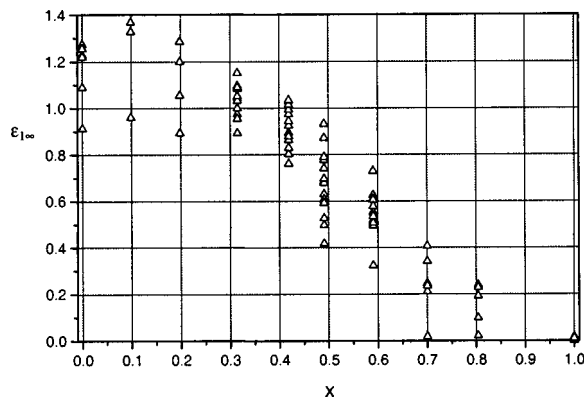
FIG. 2. Values of the $\epsilon_{1\infty}$ parameter for final objective function values which are within 5% of each other.

A. Comparison of two fitting approaches

The explanation of the fitting procedures used now follows. First, the experimental data for individual alloy compositions were fitted separately [the j in the outer sum in Eq. (13) was kept constant]. Then, the optimal cubic polynomial describing the dependence of each parameter on alloy composition x was determined. We found, however, that this procedure can significantly compromise the accuracy of the estimated dielectric function. This problem has already been noted by Terry,[20] but most authors still appear to prefer this approach. The appeal of the procedure is that it is less computationally intensive than the simultaneous fit.

The other approach is the simultaneous fit for all available alloy compositions. This procedure was more demanding on the optimization algorithm and also more computationally intensive. The number of data points has been increased by an order of magnitude, and, at the same time, the number of fitting parameters has been increased four times. Nevertheless, this computational demand can be justified for a number of reasons. First, the model parameter estimation does not give a single, unique solution to the problem. Approximations of the experimental data of similar quality can be obtained with different sets of parameters. This is illustrated in Fig. 2 showing the values of the parameter $\epsilon_{1\infty}$ obtained in different simulations. For these values of the $\epsilon_{1\infty}$ the corresponding final objective function remains within 5%. Considerable scattering of the obtained values for each alloy composition would make it difficult for one to choose the right values for the estimation of the optimal cubic polynomial describing the composition dependence of the parameter $\epsilon_{1\infty}$.

Another problem is illustrated in Fig. 3. This figure depicts three different calculated curves. The solid line is a result of the best simultaneous fit across all alloy compositions, the dotted line shows the best fit for that particular composition and the broken line shows an interesting drawback of individual fitting. The broken line was obtained using the cubic polynomial (the cubic polynomial fit to parameters obtained from individual fits) instead of parameters obtained for a particular x. The discrepancies between the broken line and the experimental data are caused by the difference between the model parameters calculated using the
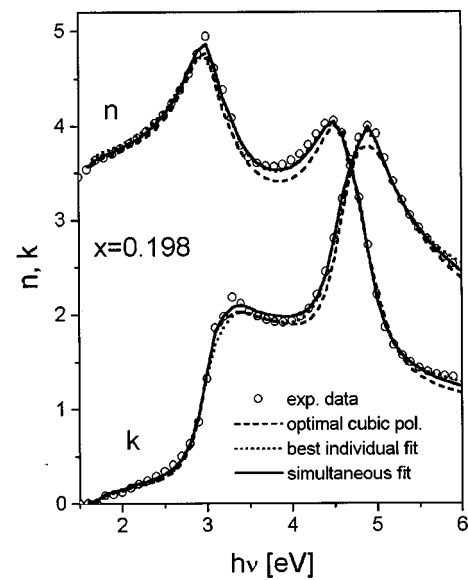

FIG. 3. The real and imaginary parts of the index of refraction for $x = 0.198$ as a function of energy; circles—experimental data, solid line—results obtained by simultaneous fit to all compositions, dotted line—best individual fit for $x = 0.198$, dashed line-results corresponding to model parameters calculated by optimal cubic polynomial approximating points obtained by fitting each composition separately.

cubic polynomial and the previously determined parameters for particular compositions. It clearly shows the deterioration of the quality of fit if the optimal cubic polynomial is found after estimating parameters for each composition separately.

The main aim of modeling the optical properties of a ternary alloy is to enable the calculation of the optical constants for alloy compositions for which there are no available experimental data. From our results it is clear that the simultaneous fitting approach is superior to individual composi-

TABLE II. Model parameter values.

| Parameter	a_{0i}	a_{1i}	a_{2i}	a_{3i}
$\epsilon_{1\infty}$	1.347	0.02	−0.568	4.210
A eV$^{1.5}$	3.06	14.210	−0.398	4.763
Γ_0 eV	0.0001	0.0107	−0.0187	0.3057
α_0	3.960	1.617	3.974	−5.413
B_1	6.099	4.381	−4.718	−2.510
B_{1s}	0.001	0.103	4.447	0.208
B_{1x} eV	1.185	0.639	0.436	0.426
B_{2x} eV	0.473	0.770	−1.971	3.384
Γ_1 eV	0.194	0.125	−2.426	8.601
α_1	0.018	0.012	0.0035	0.310
f_2 eV	4.318	0.326	4.201	6.719
Γ_2 eV	0.496	0.597	−0.282	−0.139
α_2	0.014	0.281	−0.275	−0.569
E_2 eV	4.529	4.660	0.302	0.241
f_3 eV	4.924	5.483	−0.005	−0.337
Γ_3 eV	0.800	0.434	0.572	−0.553
α_3	0.032	0.052	−0.300	0.411
E_3 eV	4.746	4.710	−0.007	−0.565
f_4 eV	3.529	4.672	−6.226	0.643
Γ_4 eV	0.302	0.414	−0.414	1.136
α_4	0.004	0.023	−0.080	0.435
E_4 eV	4.860	4.976	−0.229	0.081
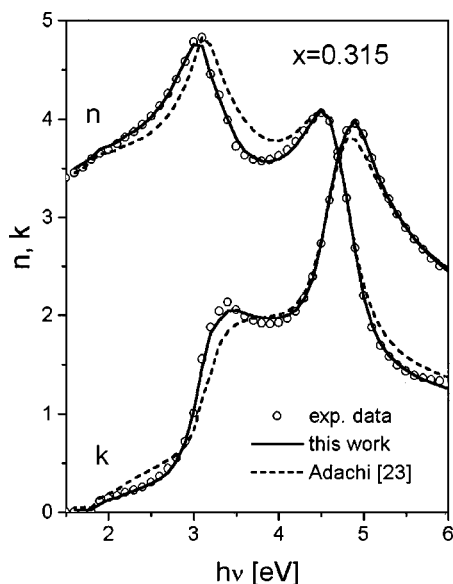
FIG. 4. Comparison with Adachi's model: the real and imaginary parts of the index of refraction vs energy for $x = 0.315$; circles—experimental data, solid line—this work, broken line—Adachi see Ref. 23.
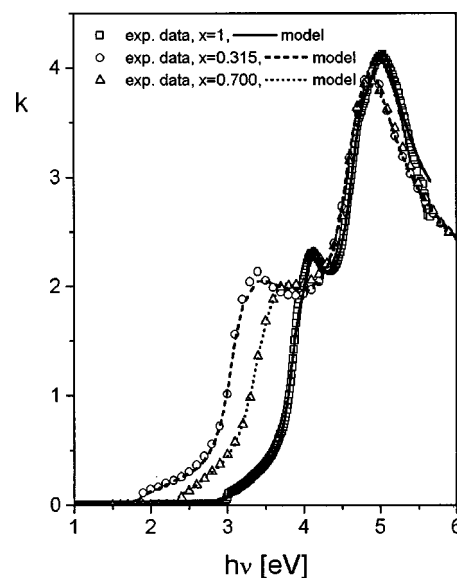

FIG. 6. The imaginary part of the index of refraction as a function of energy for compositions $x = 0.3$, 0.7, and 1.0.

tions' fitting approach. Consequently, all the data sets for all available compositions were fitted simultaneously. This produced the best cubic coefficients which minimized discrepancies between the calculated and experimental data, over the entire energy and alloy composition ranges.

B. Results

The model parameter estimation is performed as follows. Model parameters a_{0i} and a_{1i} corresponding to alloy compositions $x = 0.0$ (GaAs) and $x = 1.0$ (AlAs), respectively, are obtained first by minimizing the discrepancy between the calculated and experimental data for those compositions. The main reason for fitting these parameters separately is that

there is a greater number of experimental points over a wider spectral range for these binaries, and the data can be considered more reliable since the optical properties of these materials have been more extensively studied. After the determination of a_{0i} and a_{1i}, parameters a_{2i} and a_{3i} are obtained by minimizing the discrepancies between the calculated and experimental data for all available alloy compositions, $0 < x < 1$. The resulting coefficients are given in Table II. Excellent agreement with the experimental data is obtained for the entire investigated spectral region and for all alloy compositions.

Figure 4 gives a comparison between the model employed in this work (solid line) and the conventional Adachi's model (broken line).[23] Better agreement with experimental data is obtained in this work due to the greater
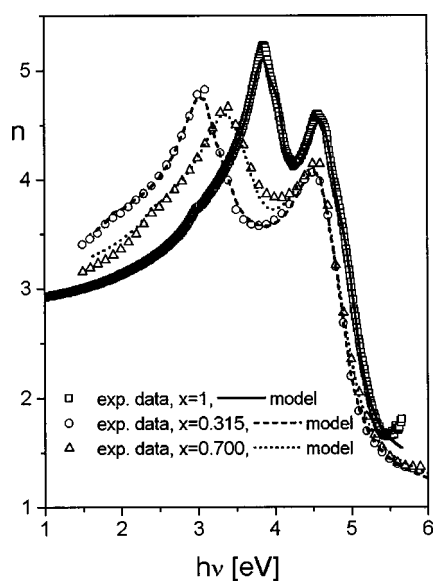

FIG. 5. The real part of the index of refraction as a function of energy for compositions $x = 0.3$, 0.7, and 1.0.
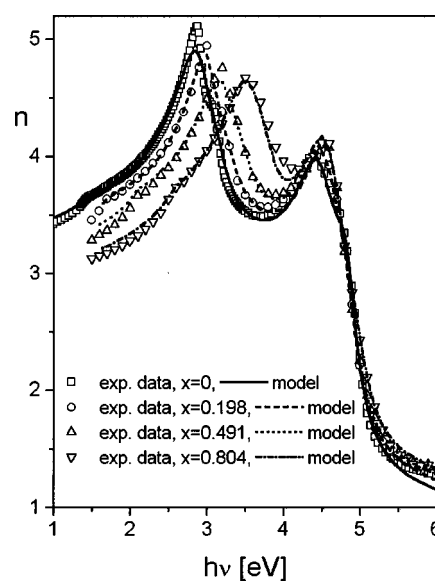

FIG. 7. The real part of the index of refraction as a function of energy for compositions $x = 0.0$, 0.2, 0.5, and 0.8.
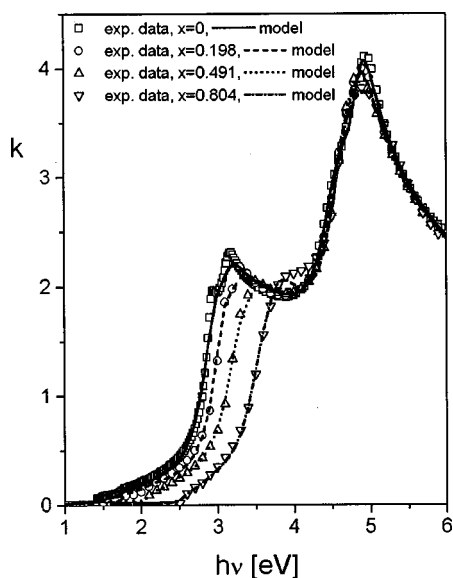
FIG. 8. The imaginary part of the index of refraction as a function of energy for compositions $x = 0.0, 0.2, 0.5,$ and 0.8.

FIG. 10. The imaginary part of the index of refraction as a function of energy for compositions $x = 0.1, 0.4,$ and 0.6.

flexibility of the model achieved by the frequency dependent damping mechanism and the inclusion of the excitonic effects. In the results presented here, we did not include the contributions of the indirect transitions, since they only exist for $x > 0.45$, and their strength should be significantly less pronounced, as they represent second-order perturbation effects. Figures 5 and 6 show the real and imaginary parts of the index of refraction versus energy, respectively, for alloy compositions 0.3, 0.7, and 1.0. Figures 7 and 8 give the energy dependence of n and k, respectively, for compositions $x = 0.0, 0.2, 0.5,$ and 0.8, while Figs. 9 and 10 show n and k versus energy for $x = 0.1, 0.4,$ and 0.6. The relative rms errors for the refractive index obtained for our model (with a total of 88 parameters) do not exceed 2.2% (2.2% for $x = 0.099$ and $x = 0.804$). However, for $x = 0.315$ and x
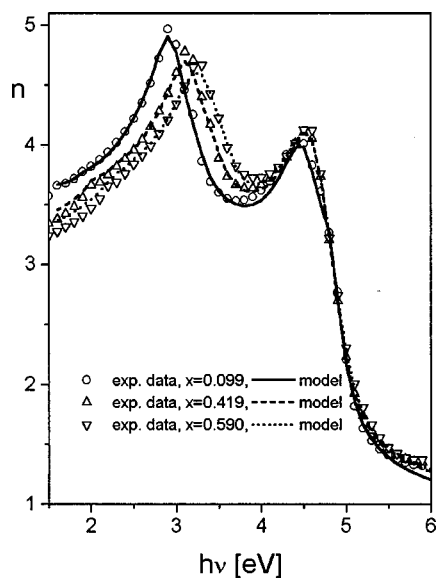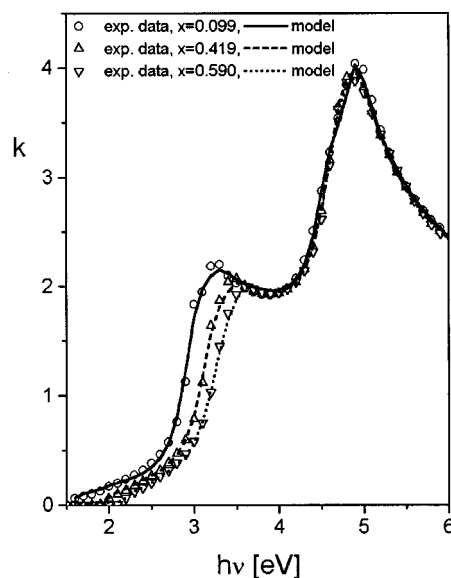
$= 0.419$ we obtain rms error as low as 1.4%. These results are comparable to the results of Kim *et al.*,[30] who obtained rms errors below 2.5% (with their model using 119 parameters), and the results of Terry,[20] who obtained rms errors below 3% (with the oscillator-based model using 144 parameters).

IV. CONCLUSION

The optical properties of $Al_xGa_{1-x}As$ are modeled in the 1.5–6 eV range for all alloy compositions, $0 \leq x \leq 1$. An extension of Adachi's model which employs the adjustable broadening function instead of the conventional Lorentzian broadening is used as described in this article. In this way greater flexibility of the model is achieved and excessive absorption resulting from the large wings of the Lorentzian line shape is eliminated. This is the main cause of inaccuracy of Adachi's model in the vicinity of the fundamental absorption edge. This article discusses the significance of employing the experimental data for all alloy compositions simultaneously when estimating the model parameters. We show that this approach yields more accurate and reliable results than those obtained by fitting each alloy composition separately. Excellent agreement with experimental data, as illustrated by reduced relative rms error for the refractive indexes (below 2.2%), is obtained in the entire investigated spectral range and for all alloy compositions. These results are obtained using 88 adjustable model parameters, which are significantly lower compared with other relevant studies.

FIG. 9. The real part of the index of refraction as a function of energy for compositions $x = 0.1, 0.4,$ and 0.6.

[1] D. E. Aspnes, S. M. Kelso, R. A. Logan, and R. Bhat, J. Appl. Phys. **60**, 754 (1986).

[2] O. J. Glembocki and K. Takarabe, in *Handbook of Optical Constants of Solids II*, edited by E. D. Palik (Academic, San Diego, 1991), pp. 513–558.

[3] S. Ozaki and S. Adachi, J. Appl. Phys. **78**, 3380 (1995).

[4] M. Garriga, M. Kelly, and K. Ploog, Thin Solid Films **223**, 122 (1993).

[5] C. M. Herzinger, H. Yao, P. G. Snyder, F. G. Celii, Y. C. Kao, B. Johs, and J. A. Woollam, J. Appl. Phys. **77**, 3416 (1995).

[6] R. E. Fern and A. Onton, J. Appl. Phys. **42**, 3499 (1971).

[7] H. C. Casey, Jr., D. D. Sell, and M. B. Panish, Appl. Phys. Lett. **24**, 63 (1974).

[8] S. H. Wemple and M. DiDomenico, Jr., Phys. Rev. Lett. **23**, 1156 (1969).

[9] S. H. Wemple and M. DiDomenico, Jr., Phys. Rev. B **3**, 1338 (1971).

[10] M. A. Afromowitz, Solid State Commun. **15**, 59 (1974).

[11] D. Campi and C. Papuzza, J. Appl. Phys. **57**, 1305 (1985).

[12] J. H. Shin and Y. H. Lee, J. Appl. Phys. **76**, 8048 (1994).

[13] J. J. Dudley, D. L. Crawford, and J. E. Bowers, IEEE Photonics Technol. Lett. **PTL-4**, 311 (1992).

[14] D. H. Christensen, J. G. Pellegrino, and R. G. Hickernell, J. Appl. Phys. **72**, 5982 (1992).

[15] D. Babic, Y. Chung, and N. D. J. E. Bowers, IEEE J. Quantum Electron. **QE-29**, 1950 (1993).

[16] Z. M. Chuang and L. A. Coldren, IEEE J. Quantum Electron. **QE-29**, 1071 (1993).

[17] Z. M. Chuang, M. J. Mondry, D. B. Young, D. A. Cohen, and L. A. Coldren, Appl. Phys. Lett. **63**, 880 (1993).

[18] S. Y. Hu, S. W. Corzine, Z. M. Chuang, K. K. Law, D. B. Young, A. C. Gossard, L. A. Coldren, and J. L. Merz, Appl. Phys. Lett. **66**, 2040 (1995).

[19] M. Erman, J. B. Theeten, P. Chambon, S. M. Kelso, and D. E. Aspnes, J. Appl. Phys. **56**, 2664 (1984).

[20] F. L. Terry, Jr., J. Appl. Phys. **70**, 409 (1991).

[21] S. Adachi, J. Appl. Phys. **53**, 5863 (1982).

[22] S. Adachi, J. Appl. Phys. **58**, R1 (1985).

[23] S. Adachi, Phys. Rev. B **38**, 12345 (1988).

[24] D. W. Jenkins, J. Appl. Phys. **68**, 1848 (1990).

[25] S. Adachi, T. Kimura and N. Suzuki, J. Appl. Phys. **74**, 3435 (1993).

[26] R. J. Deri and M. A. Emanuel, J. Appl. Phys. **74**, 3435 (1993).

[27] Y. Kokubo and I. Ohto, J. Appl. Phys. **81**, 2042 (1997).

[28] J. Zheng, C.-H. Lin, and C. H. Kuo, J. Appl. Phys. **82**, 792 (1997).

[29] C. C. Kim, J. W. Garland, H. Abad, and P. M. Raccah, Phys. Rev. B **45**, 11749 (1992).

[30] C. C. Kim, J. W. Garland, H. Abad, and P. M. Raccah, Phys. Rev. B **47**, 1876 (1993).

[31] C. C. Kim and S. Sivananthan, J. Appl. Phys. **78**, 4003 (1995).

[32] O. Stenzel, R. Petrich, W. Scharff, A. Tikhonravov, and V. Hopfe, Thin Solid Films **207**, 324 (1992).

[33] A. Franke, A. Stendal, O. Stenzel, and C. von Borczyskowski, Pure Appl. Opt. **5**, 845 (1996).

[34] A. D. Rakić and M. L. Majewski, J. Appl. Phys. **80**, 5509 (1996).

[35] A. D. Rakić, J. M. Elazar, and A. B. Djurišić. Phys. Rev. E **52**, 6862 (1995).

[36] A. B. Djurišić, A. D. Rakić, and J. M. Elazar, Phys. Rev. E **55**, 4797 (1997).